Stress transfer along the western boundary of the Bayan Har Block on the Tibet Plateau from the 2008 to 2020 Yutian earthquake sequence in China

Ke Jia[1*], Shiyong Zhou[2*], Jiancang Zhuang[3], Changsheng Jiang[4]

1 School of Automation, Northwestern Polytechnical University, Xi'an 710129, China

2 School of Earth and Space Sciences, Peking University, Beijing 100871, China

3 The Institute of Statistical Mathematics, 10-3 Midori-Cho, Tachikawa, Tokyo 190-8562, Japan

4 Institute of Geophysics, China Earthquake Administration, No.5 Minzu Daxue Nan Road, Haidian District, Beijing 100086, China

*Corresponding authors: jk@nwpu.edu.cn, zsy@pku.edu.cn

Key points:

1. Four Ml>=6.0 have occurred on the western boundary of the Bayan Har block, NW Tibet, China, from 2008 to 2020.
2. The 2008 Yutian earthquake may have contributed to the occurrences of the 2014 and 2020 Yutian events due to stress triggering.
3. Statistical insights provide a good cross reference for the triggering mechanism due to small uncertainties.

Abstract

Eight Ml≥7.0 earthquakes have occurred around the Bayan Har block, NW Tibet, China, since 2000, resulting in a large number of casualties and countless economic loss. Near the western boundary of the Bayan Har block, four Ml≥6.0 Yutian earthquakes have occurred from 2008 to 2020. Stress interactions among them are comprehensively investigated by applying the ETAS (Epidemic-Type Aftershock Sequence) model and calculating ΔCFS (Coulomb failure stress change). The viscoelastic ΔCFS induced by proceeding Yutian earthquakes on hypocenters of the 2012, 2014 and 2020 Yutian earthquakes are -1.5004×10^{-4}, 3.5820×10^{-3} and 1.4770×10^{-1} MPa, respectively. The background probabilities of the 2008, 2012, 2014 and 2020 Yutian earthquakes are 0.87, 0.97, 1.5×10^{-3} and 8.7×10^{-5}, respectively. Combining those two independent approaches, we conclude that the 2008 and 2012 Yutian earthquakes are more like background earthquakes and that the 2014 and 2020 Yutian earthquakes were triggered by the proceeding Yutian earthquakes.

Plain Language Summary

Along the boundaries of the Bayan Har block, NW Tibet, China, there have been eight large earthquakes since 2000, resulting in a large number of casualties and countless economic loss. At its western boundary (Yutian region), four earthquakes with local magnitudes larger than 6.0 have occurred since 2008. Whether these four large earthquakes were triggered is an important question in assessing regional seismic hazards. We combine two methods to address this issue. One is direct calculation of stress transfer and the other is estimation of the probabilities of them being background events (an event is driven by tectonic loading). We find that the stress transfer from proceeding major earthquakes to the 2012 Yutian earthquake is smaller than the earthquake triggering threshold (0.01 MPa), while those of the 2014 and 2020 Yutian earthquakes were moderate compared with the triggering threshold. The background probabilities of the 2008 and 2012 Yutian earthquakes are high (close to 1.0), while background probabilities of the 2014 and 2020 Yutian earthquakes are very low (close to 0.0). Thus, we conclude that the 2008 and 2012 Yutian earthquakes are more like background earthquakes and that the 2014 and 2020 Yutian earthquakes were triggered by the proceeding Yutian earthquakes.

1. Introduction

Stress interactions among major earthquakes have received increasing attention. A number of case studies (e.g., the 1992 Landers and 1999 Hector Mine earthquakes in the US (*Freed and Lin*, 2001); the 2008 Wenchuan, 2013 Lushan and 2017 Jiuzhaigou earthquakes in China (*Jia et al.*, 2014; *Jia et al.*, 2018; *Wan and Shen*, 2010; *Wang et al.*, 2014b); the 2010-2011 Canterbury Earthquake Sequence in New Zealand (*Quigley et al.*, 2016); and the foreshock and mainshock of the 2019 Ridgecrest earthquake in the US (*Pope and Mooney*, 2020; *Ramos et al.*, 2020)) have been investigated under the framework of the Coulomb failure hypothesis, which assumes that positive ΔCFS promotes the occurrence of earthquakes and negative ΔCFS delays them. In addition, many researchers have shown that the calculated ΔCFS are positively correlated with observed seismicity rate changes (*Harris*, 1998; *Jia et al.*, 2014; *Kroll et al.*, 2017; *Pollitz and Cattania*, 2017; *Stein*, 1999; *Toda et al.*, 2012; *Toda et al.*, 2005; *Zhuang et al.*, 2005). This indicates that observed seismicity increases in regions with positive ΔCFS and decreases in regions with negative ΔCFS values. However, several studies have found that earthquakes still occurred in a stress shadow (*Harris and Simpson*, 1996; *Jia et al.*, 2018; *Parsons*, 2002), which cannot be explained by the Coulomb failure hypothesis. Earthquake triggering mechanisms have also been investigated in previous studies (*Freed*, 2005). Coseismic slip (*McCloskey et al.*, 2005), postseismic deformation (e.g., afterslip (*Cattania et al.*, 2015), viscoelastic relaxation of the lower crust and upper mantle (*Freed and Lin*, 2001)), dynamic seismic waves (*Gomberg et al.*, 2001) and fluid-involved processes (e.g., poroelastic rebound) (*Hughes et al.*, 2010; *Tung and Masterlark*, 2018) could contribute to triggering earthquakes. Remote triggering of earthquakes at great distances could be well explained by dynamic triggering due to the passage of seismic waves, while distinguishing local triggering in the near field between static and dynamic stress changes could be a challenge (*Meng and Peng*, 2014). In this way, calculations of ΔCFS and seismicity rate changes could help to clarify stress interactions between earthquakes and faults and further evaluate seismic hazards.

The recent June 26 (GMT+8), 2020 Mw 6.3 Yutian earthquake (hereafter 20YT) occurred in the western Kunlun Mountains, NW Tibet, China. Three other M≥6.0 earthquakes have

87 occurred near the epicenter of the 20YT since 2008. The March 20, 2008 Mw 7.1 Yutian
88 earthquake (hereafter 08YT), one of the largest normal earthquakes on the continents, occurred
89 94 km to the west of the epicenter of the 20YT. The August 12, 2012 Mw 6.2 Yutian earthquake
90 (hereafter 12YT) and the February 12, 2014 Mw 6.9 Yutian earthquake (hereafter 14YT)
91 occurred 25 km and 61 km to the north of the epicenter of the 20YT (Figure 1). The source
92 region of these four earthquakes on the western boundary of the Bayan Har block experiences
93 an extensive stress field bounded by two strike-slip fault systems: the Altyn Tagh fault in the
94 north and the Longmu-Gozha Co fault in the south (*Taylor and Yin*, 2009), which further relates
95 to the collision of the Indian plate and Eurasian plate. This area is the intersection of multiple
96 groups of large strike-slip active fault belts with different strikes. The 08YT, 12 YT, 14 YT and
97 20YT sequences provide an opportunity for a case study of the Coulomb failure hypothesis and
98 help to evaluate the seismic hazard of the Bayan Har block.
99

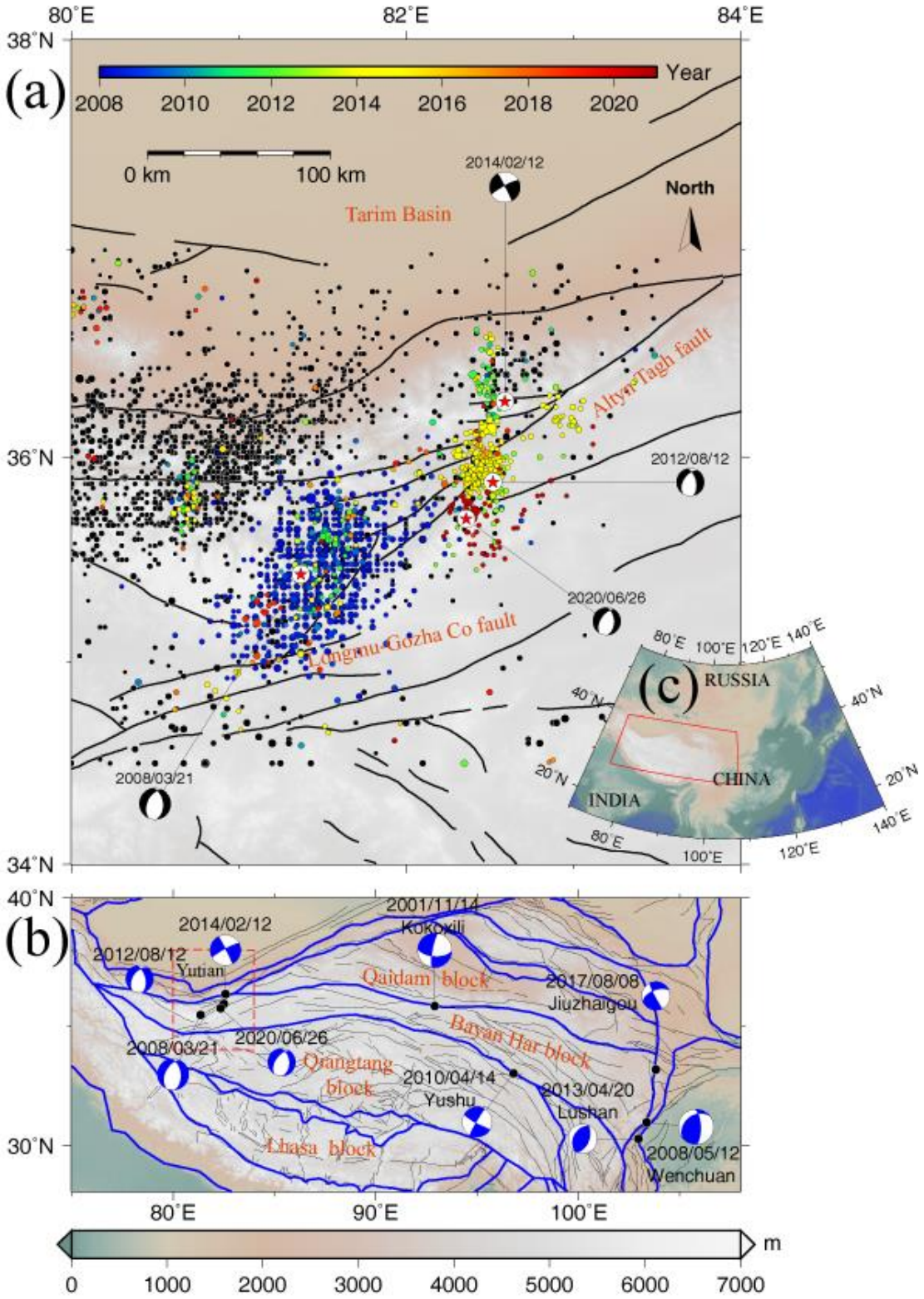

Figure 1 Tectonic settings of the Yutian region and Bayan Har block. (a) The black filled circles represent earthquakes with M≥3.5 from 1 January 1970 to 31 December 2007 (from China Earthquake Data Center, http://data.earthquake.cn/index.html). The color filled circles are earthquakes with M≥3.5 from 1 January 2008 to 23 August 2020, and colors represent their

105 occurrence time. The four red stars represent the epicenters of the 2008, 2012, 2014 and 2020
106 Yutian earthquakes, and their focal mechanisms are from the Global Centroid Moment Tensor
107 (GCMT, https://www.globalcmt.org/CMTsearch.html). The black lines represent major faults
108 (*Zhang et al.*, 2003). (b) Nine major earthquakes (M≥7.0 except for the Yutian region) have
109 occurred on the boundaries of the Bayan Har block since 2000. The red dashed polygon
110 represents the region of (a). (c) The red solid polygon represents the region of (b) with respect
111 to mainland China.
112
113 Previous studies have shown stress triggering between the 08YT and 14YT (*Li et al.*, 2015;
114 *Wang et al.*, 2017; *Zhao et al.*, 2016) and seismicity rate changes following the 08YT, 12YT
115 and 14YT (*Jiang et al.*, 2014; *Zhao et al.*, 2016). Using a three-dimensional viscoelastic finite
116 element model, *Li et al.* (2015) showed that ΔCFS induced by the 08YT on the slip direction
117 of the 14YT exceeded 0.01 MPa (the earthquake triggering threshold) (*Harris*, 1998;
118 *Reasenberg and Simpson*, 1992). They implied an apparent triggering effect of the 08YT to
119 14YT and suggested that the 14YT had advanced 21.4-24.9 years from the 08YT (*Li et al.*,
120 2015). *Zhao et al.* (2016) claimed that the 14YT was located in the triggering zone caused by
121 the 08YT, and the observed spatial distributions of aftershocks of these two major events were
122 well correlated with positive ΔCFS distribution. *Wang et al.* (2017) examined coseismic,
123 postseismic and interseismic ΔCFS induced by the 08 YT on the 14 YT hypocenter and found
124 a triggering relationship between them. *He et al.* (2020) calculated the coseismic ΔCFS from
125 the 08YT, 12YT and 14YT and found that the 20YT falls in the positive Coulomb stress region,
126 suggesting that previous events promoted the 20YT.
127
128 However, the roles of the 12YT in stress interactions with other Yutian earthquakes and
129 postseismic stress changes on the hypocenter of the 20YT have not been investigated. More
130 importantly, whether the occurrence of the 20YT was triggered by proceeding Yutian
131 earthquakes or a background event may lead to different evaluations of regional seismic hazards.
132 If the 20YT was a triggered event, the local stress level may still be in a condition of postseismic
133 release or adjustment. On the other hand, an independent 20YT implies continuous tectonic

loading and release. Especially for a relatively small region, occurrences of four M≥6.0 earthquakes within 13 years are rare and provide an opportunity to study static stress interactions (elastic and viscoelastic stress changes) among them. Furthermore, together with seismicity analysis, these two independent kinds of evidence could be useful to understand the occurrence of the 20YT and seismic hazards in the Bayan Har block.

In this study, we comprehensively investigate the seismicity rate changes in the Yutian region from 2008 to 2020, the ΔCFS at the hypocenter of the 20YT induced by the proceeding Yutian earthquakes (08YT, 12YT and 14YT), and the correlations between them. The ETAS model and stochastic declustering method are used to obtain the background seismicity rate change. The coseismic (elastic) and postseismic (viscoelastic) ΔCFS are calculated in an elastic/viscoelastic layered half-space. The uncertainties of ΔCFS are investigated by considering different friction coefficients. Based on the results of ΔCFS and seismicity analysis, we infer that the 08YT may have contributed to the occurrence of the 14YT and 20YT due to stress triggering.

2. Detection of seismicity rate changes by using the ETAS model

2.1 Space-time ETAS model

The space-time ETAS model, proposed by *Ogata* (1998), combines several classic statistical laws in seismicity, including the Omori-Utsu law, productivity law and Gutenberg-Richter law. The ETAS model assumes that each earthquake could trigger its own aftershocks with an ability corresponding to its magnitude. The ETAS model has been successfully applied in many regions and has become a standard model to analyze spatial and temporal seismicity (*Jia et al.*, 2014; *Jia et al.*, 2018; *Ogata*, 2004; *Ogata and Zhuang*, 2006; *Zhuang et al.*, 2005; *Zhuang et al.*, 2004). Details of the space-time ETAS model can be found in *Ogata and Zhuang* (2006).

After obtaining final estimations of parameters of the ETAS model, the background probability (an event is regarded as a background event with a probability) of the jth event φ_j, can be estimated by

$$\varphi_j = \frac{\mu\left(x_j, y_j\right)}{\lambda\left(t_j, x_j, y_j\right)}, \quad (1)$$

where $\mu\left(x_j, y_j\right)$ is the background and total seismicity rate at the location of *j*th event and $\lambda\left(t_j, x_j, y_j\right)$ is the total seismicity rate at the location and occurrence time of *j*th event.

2.2 Fitting ETAS model

The catalog used in this study was downloaded from the China Earthquake Data Center (CEDC, http://data.earthquake.cn/index.html). A polygon region (80.0°-83.5°E, 34.5°-37.0°N) is selected to present the Yutian region for model fitting and seismicity analysis, and events above the cutoff magnitude were selected within the spatiotemporal range to fit the ETAS model by the maximum likelihood method. The time range is from 1 January 1980 to 23 August 2020, and the complete magnitude is approximately 3.5 from 1980 to 2020 (Figure S2), and we set the cutoff magnitude to 3.5. Details of the complete magnitude check are presented in the Supporting Information. The final estimations of the model parameters for the Yutian region are $\hat{A} = 0.382$ (events), $\hat{c} = 0.037$ (day), $\hat{\alpha} = 1.163$ (m^{-1}), $p = 1.178$, $\hat{D} = 1.46 \times 10^{-2}$ (deg^2), $\hat{q} = 2.396$, and $\hat{\gamma} = 0.211$ (m^{-1}).

2.3 Background seismicity rate in the Yutian region

The background probabilities of earthquakes with Mw≥6.0 are listed in Table S1, and the spatiotemporal distributions of the background probabilities are shown in Figure S3. From Figure S3, a number of aftershocks have been effectively distinguished. The spatiotemporal distributions of background probabilities are not sensitive to different intervals of background probabilities (Figure S3a-S3d). The background probabilities of 08YT, 12YT, 14YT and 20YT are 0.87, 0.97, 1.5×10^{-3} and 8.7×10^{-5}, respectively. This implies that the 08YT and 12YT are more like background earthquakes and that the 14YT and 20YT are triggered events in view of the ETAS model.

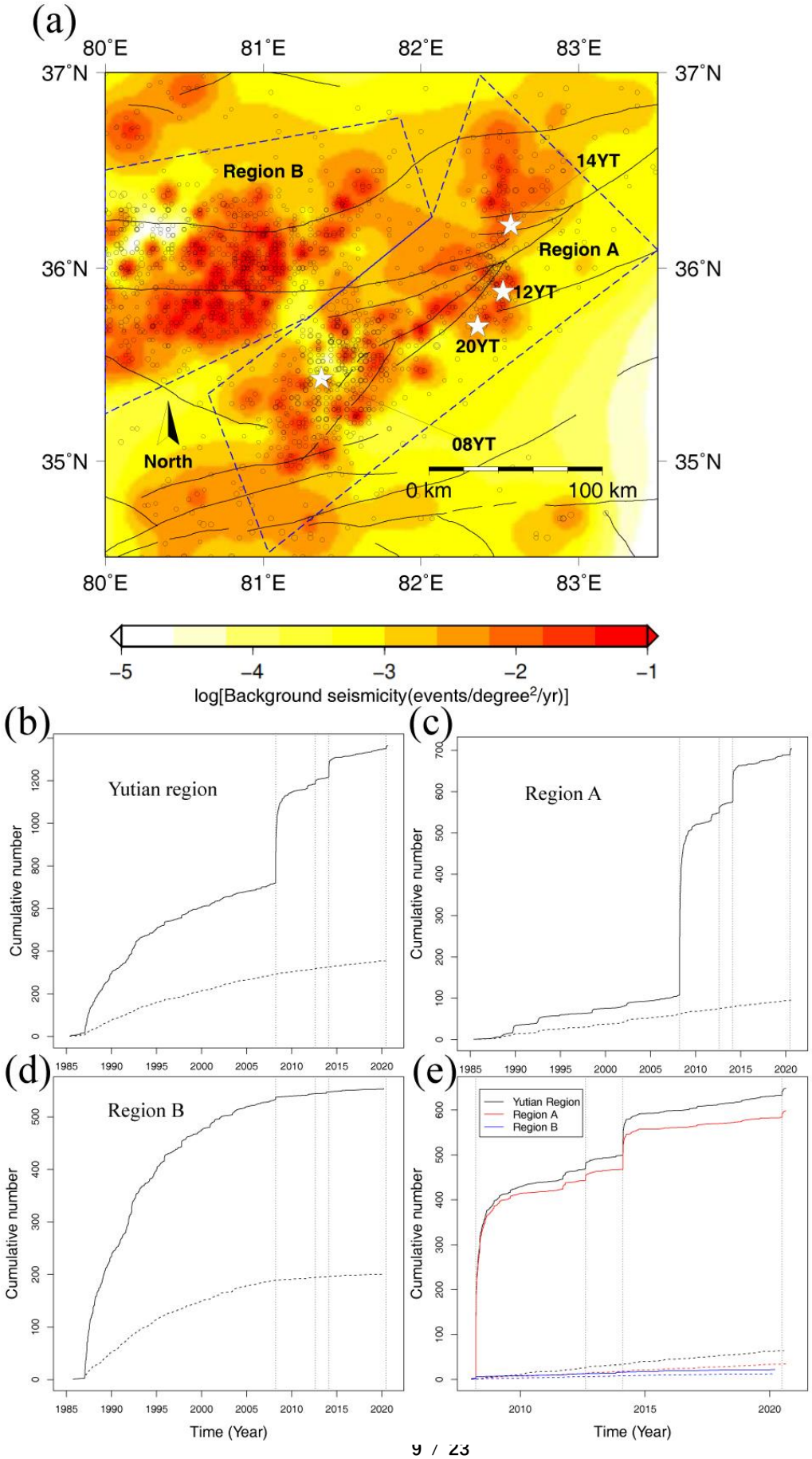
(a)
80°E
81°E
82°E
83°E
37°N
36°N
35°N
Region B
14YT
Region A
12YT
20YT
08YT
North
0 km
100 km
−5
−4
−3
−2
−1
log[Background seismicity(events/degree²/yr)]
(b)
Yutian region
Cumulative number
(c)
Region A
Cumulative number
(d)
Region B
Cumulative number
Time (Year)
(e)
Yutian Region
Region A
Region B
Cumulative number
Time (Year)

Figure 2 (a) Estimated spatial background seismicity in the Yutian region. Black circles represent earthquakes with magnitudes larger than 3.5 from 1970 to 2020. Four white stars indicate the 08YT, 12YT, 14YT and 20YT. Black lines are active faults. Regions A and B are marked with blue dashed lines for seismicity analysis. Note that the background seismicity rate is represented by the logarithm scale. (b)-(e) Cumulative number of earthquakes and background probabilities for the Yutian region (b), region A (c) and region B (d) marked in Figure 2(a). (e) A zoomed in view of seismicity changes from 2008 to 2021. The solid lines represent cumulative numbers of earthquakes in the study region and the dashed line represents the cumulative number of background probabilities. The four vertical dashed lines indicate the occurrence times of the 08YT, 12YT, 14YT and 20YT from left to right.

The spatial background seismicity is shown in Figure 2a. The epicenters of the 08YT, 12YT, 14YT and 20YT suffer the highest background seismicity (approximately 0.1 M≥3.5 events/degree^2/yr), where the fault traces are also dense. The spatial background seismicity in the Yutian region shows a relatively high level resulting from the complex stepover zone with multiple normal faults (*Bie and Ryder*, 2014; *Tapponnier et al.*, 2001; *Xu et al.*, 2013).

The cumulative background probabilities of earthquakes $S(t)$, proposed by *Zhuang et al.* (2005), are written as

$$S(t) = \sum_{t_j < t} \varphi_j \tag{2}$$

We assume that the background seismicity rate is time-invariant in a stable region, thus $S(t)$ constantly increases with time. Changes in the slope of the $S(t)$ curve imply changes in the background seismicity rate: an increased slope represents an activation of the background seismicity and a decreased slope indicates background quiescence.

Figure 2b-2e shows the cumulative number of earthquakes and background probabilities in the Yutian region and two subregions marked in Figure 2a. From **错误!未找到引用源。**a Figure 2b-2e, it can be seen that the cumulative number of earthquakes in the Yutian region

dramatically increases after each major earthquake, while the rate of background probability remained stable from 1990 to 2020 and was not affected by the major earthquakes. This finding suggests that the Yutian region experiences constant background seismicity under a stable tectonic environment. The relationship between these four major Yutian earthquakes will be discussed later along with the calculations of ΔCFS . Region A indicates the fault zone of these four Yutian earthquakes, experiencing a constant background seismicity rate (**错误!未找到引用源。**Figure 2c). Region B shows a decrease in background seismicity after the 08YT, which may have bene caused by a negative ΔCFS induced by the 08YT (Figure 3a and 3d).

3. Coulomb Failure Stress change

To further investigate the stress interaction among the 2008, 2012, 2014 and 2020 Yutian earthquakes, we calculate the static (coseismic) and viscoelastic (postseismic) Coulomb stress changes induced by the proceeding events using the numerical method of *Wang et al.* (2006). The lower crust and upper mantle are considered to be layered and viscoelastic. The proposed 3D viscoelastic model contains an elastic upper crust, a viscoelastic lower crust with a viscosity of $1\times10^{18}Pa\bullet s$ and a viscoelastic upper mantle with a viscosity value of $1\times10^{20}Pa\bullet s$ (*Jia et al.*, 2012; *Wang et al.*, 2006; *Xiong et al.*, 2010). The layered rheological structure of the lithosphere is presented in the Supporting Information (Figure S4).

3.1 Method of calculation of ΔCFS

Given the shear stress change $\Delta\tau$ (positive in the sense of motion of the relevant fault) and the normal stress change $\Delta\sigma$ (positive for extension), ΔCFS can be calculated by (*Harris*, 1998; *Steacy et al.*, 2005),

$$\Delta CFS = \Delta\tau + \mu\left(\Delta\sigma - \left(\beta/3\right)\sum\Delta\tau_{ii}\right) \tag{3}$$

where μ is the friction coefficient and β is Skempton's coefficient. If the medium is homogeneous and the fault zone materials are ductile, as discussed in *Harris* (1998) (formulas (3), (4) and (5) therein), ΔCFS can simply be calculated using

$$\Delta CFS = \Delta\tau + \mu'\Delta\sigma \tag{4}$$

where μ' is the apparent coefficient of friction and $\mu' = \mu(1-\beta)$.

Notably, the joint static and viscoelastic stress changes induced by the 2008/2012/2014 Yutian earthquakes are considered in this study. Other possible mechanisms (e.g., dynamic stress changes, stress changes driven by afterslips or fluid emigration), which may also contribute to seismicity rate changes, have been neglected. The main mechanisms of postearthquake deformation include viscoelastic relaxation of the lower crust and upper mantle and postseismic afterslip on the fault plane. In the near field and the short period after the mainshock, the postseismic deformation mainly comes from afterslip relaxing the stress perturbation by localized deformation in the region of the fault plane (*Agata et al.*, 2019; *Helmstetter and Shaw*, 2009). In the far field and longterm after the mainshock, the viscoelastic relaxation of the lower crust and upper mantle has a more significant contribution to postseismic deformation (*He et al.*, 2018; *Masuti et al.*, 2016; *Nur and Mavko*, 1974; *Peña et al.*, 2020). Because of the long distances between the epicenter of the 08YT and the epicenters of the other three Yutian earthquakes, the contribution of afterslips induced by the 08YT is smaller than that of viscoelastic relaxation of the lower crust and upper mantle. Poroelastic rebound, which refers to coseismic stress changes that drive fluid flow from undrained conditions to drained conditions, may also alter the local stress field after a major earthquake (*Freed*, 2007). However, previous studies have shown that poroelastic rebound usually occurs within several months (*Hughes et al.*, 2010; *Jonsson et al.*, 2003; *Tung and Masterlark*, 2018) and its contribution is smaller than that of afterslip and viscoelastic relaxation processes (*Peña et al.*, 2020; *Wang and Fialko*, 2018). Dynamic triggering due to the passage of seismic waves occurs hours and days after the mainshock (*Freed*, 2005; *Gomberg et al.*, 2001; *Hill and Prejean*, 2007). Thus, the poroelastic rebound process and dynamic triggering have been neglected in our study due to much longer time intervals between these four Yutian earthquakes (4 to 12 years). In addition, the impact of power-law rheology on viscoelastic relaxation has been investigated in recent years (*Agata et al.*, 2019; *Liu et al.*, 2021; *Peña et al.*, 2019; 2020), and we apply linear viscoelastic rheology in this study for simplicity. The application of power-law rheology needs further investigation and is beyond our aims in this study.

3.2 Stress interactions among the four Yutian earthquakes

We have comprehensively investigated stress transfer among the 08YT, 12YT, 14YT and 20YT, which indicates that both static and viscoelastic ΔCFS induced by the proceeding Yutian earthquakes are calculated at the hypocenters of later Yutian earthquakes (Table 1). The coseismic slip model of the 2008 Yutian earthquake, provided by *Elliott et al.* (2010), is jointly inverted by the InSAR and body wave data. The coseismic slip model of the 2014 Yutian earthquake is estimated by inverting teleseismic data (*Zhang et al.*, 2014). The synthetic slip model 2012 Yutian earthquake is estimated based on the empirical relations of *Wells and Coppersmith* (1994) because of the lack of published coseismic slip models. The resolving depths of the 12YT, 14YT and 20YT are 15 km, 20 km and 15 km, respectively. The project planes are selected from focal mechanisms of the GCMT. The friction coefficient is set to 0.4, and Skempton's coefficient is set to 0.5.

Table 1 ΔCFS of the four major Yutian earthquakes (MPa)

	08YT		12YT		14YT		Proceeding Yutian earthquake
	coseismic	viscoelastic	coseismic	viscoelastic	coseismic	viscoelastic	Combined*
12YT	1.0×10^{-3}	-1.5×10^{-4}	\	\	\	\	-1.5×10^{-4}
14YT	-7.5×10^{-3}	2.6×10^{-3}	3.1×10^{-4}	9.6×10^{-4}	\	\	3.6×10^{-3}
20YT	3.0×10^{-3}	7.3×10^{-3}	3.5×10^{-2}	3.5×10^{-2}	1.1×10^{-1}	1.1×10^{-1}	1.5×10^{-1}

*"Combined" indicates coseismic and viscoelastic ΔCFS induced by the three proceeding Yutian earthquakes.

From Table 1, at the hypocenter of the 12YT, the static and viscoelastic ΔCFS induced by 08YT are smaller (approximately 10^{-3} to 10^{-4} MPa) than the triggering threshold (0.01 MPa), implying that the stress interaction between these two events is weak. At the hypocenter of the 14YT, the static and viscoelastic ΔCFS induced by the 08YT (0.0036 MPa) are smaller than

298 the triggering threshold (0.01 MPa), which implies a weak interaction. The static and
299 viscoelastic ΔCFS induced by the 12YT on the 14YT are insignificant (approximately 10^{-4}
300 MPa), implying that the stress interaction between them is very weak. For the 20YT, the
301 ΔCFS induced by the 08YT is small (approximately 10^{-3} MPa), the ΔCFS induced by the
302 12YT is larger (approximately 10^{-2} MPa) than the triggering threshold, and the ΔCFS induced
303 by the 14YT is noticeable (approximately 10^{-1} MPa). These findings imply that the proceeding
304 Yutian earthquakes contributed to the occurrence of the 20YT. The largest triggering
305 contribution comes from the 14YT (approximately 71%≈0.10523/0.1477).
306

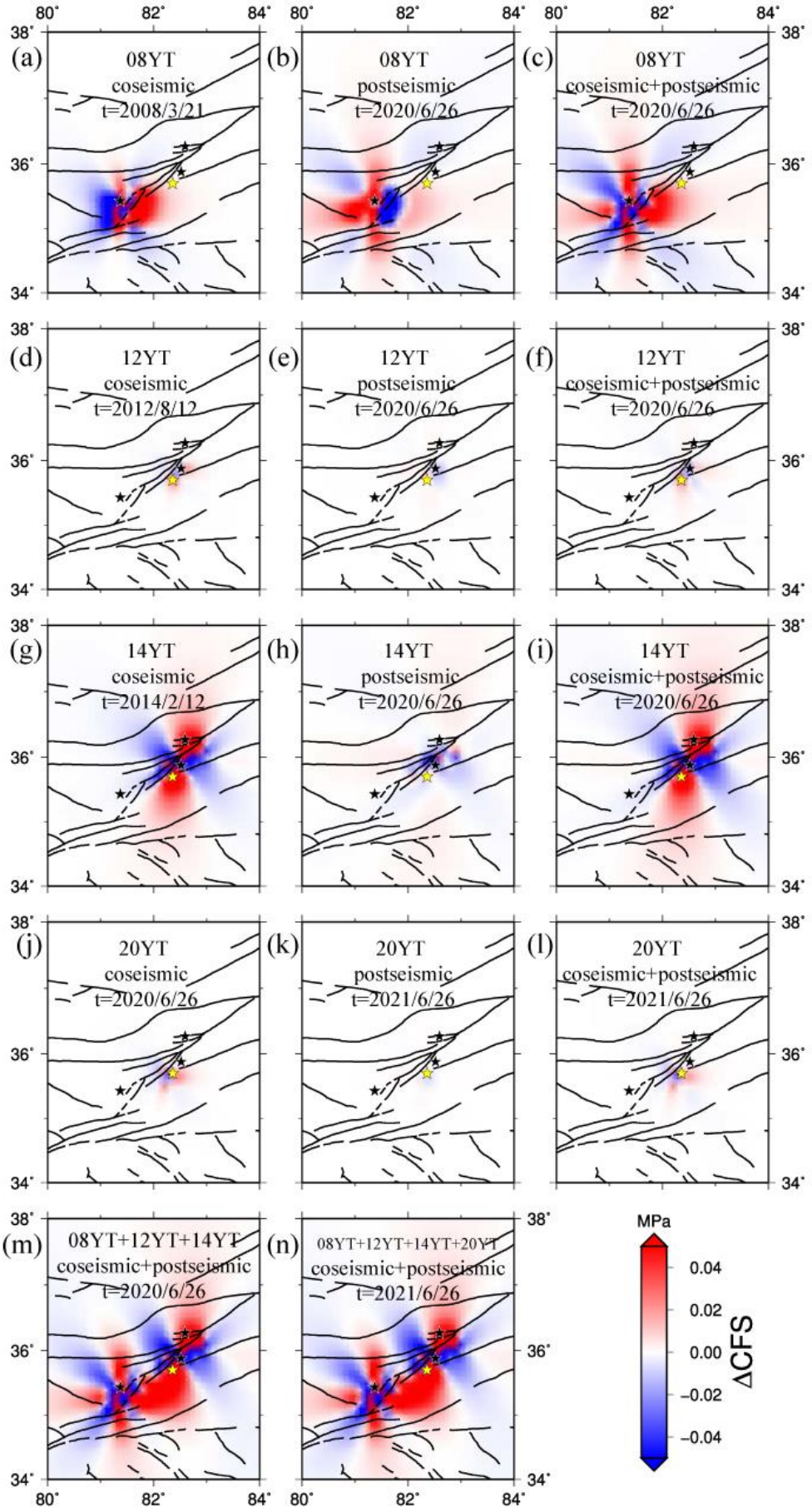
(a)
08YT
coseismic
t=2008/3/21
(b)
08YT
postseismic
t=2020/6/26
(c)
08YT
coseismic+postseismic
t=2020/6/26
(d)
12YT
coseismic
t=2012/8/12
(e)
12YT
postseismic
t=2020/6/26
(f)
12YT
coseismic+postseismic
t=2020/6/26
(g)
14YT
coseismic
t=2014/2/12
(h)
14YT
postseismic
t=2020/6/26
(i)
14YT
coseismic+postseismic
t=2020/6/26
(j)
20YT
coseismic
t=2020/6/26
(k)
20YT
postseismic
t=2021/6/26
(l)
20YT
coseismic+postseismic
t=2021/6/26
(m)
08YT+12YT+14YT
coseismic+postseismic
t=2020/6/26
(n)
08YT+12YT+14YT+20YT
coseismic+postseismic
t=2021/6/26
80°
82°
84°
38°
36°
34°
MPa
0.04
0.02
0.00
−0.02
−0.04
ΔCFS

307

Figure 3 Spatial distribution of ΔCFS at the hypocenter of the 20YT induced by the four Yutian earthquakes. (a), (d), (g) and (j) show static (coseismic) ΔCFS induced by the 08YT, 12YT, 14YT and 20YT. (b), (e), (h) and (k) show postseismic ΔCFS induced by the 08YT, 12YT, 14YT and 20YT. (c), (f), (i) and (l) show the combined (coseismic and postseismic) ΔCFS induced by the 08YT, 12YT, 14YT and 20YT. (m) Combined ΔCFS induced by all three proceeding Yutian earthquakes (08YT, 12YT and 14YT). (n) Combined ΔCFS induced by all four Yutian earthquakes (08YT, 12YT, 14YT and 20YT) after one year of occurrence of 20YT. The black lines represent major faults, black stars indicate 08YT, 12YT and 14YT, and yellow star shows location of 20YT. The resolving depth is 15 km and the strike, dip, and rake angles are 213°, 52°, and -66° (GCMT), respectively.

The triggering contribution from the 08YT, 12YT and 14YT to the 20YT can also be clearly identified from the spatial distribution of ΔCFS (Figure 3). From Figure 3a-3g, the epicenter of the 20YT always falls into the positive zone of ΔCFS, which is similar to the results of *He et al.* (2020). *He et al.* (2020) only calculated coseismic ΔCFS; the spatial distribution of ΔCFS induced by the 08YT, 12YT and 14YT (Figure 12 in their paper) is different in this study (Figure 3m and 3n) in several regions, which are dominated by a large postseismic ΔCFS from the 08YT (Figure 3b). The uncertainties of ΔCFS impacted by resolving depth, receiver fault parameters and friction coefficient are also investigated in the Supplementary Information (Tables S2-S3, Figures S5-S7), and the results are similar. The 08YT and 14YT generated a wider spatial stress disturbance than the 12YT due to their larger magnitudes. It is also interesting that several faults between the epicenters of 08YT and 20YT experience a positive ΔCFS induced by the 08YT and a negative ΔCFS induced by the 14YT at the same time. The seismic hazard in this region may receive more research attention.

4. Discussion

4.1 Uncertainties of calculations of ΔCFS

Large uncertainties in the calculations of ΔCFS caused by nonunique solutions of the source slip distribution and poorly constrained parameters (e.g., friction coefficient and resolving

depth) may weaken the results based on ΔCFS (*Jia et al.*, 2018; *Steacy et al.*, 2004; *Wang et al.*, 2014a). *Jia et al.* (2018) have shown that large uncertainties in ΔCFS may lead to different or even conflicting results in the case of the 2008 Wenchuan and 2017 Jiuzhaigou earthquakes in China. One way to minimize uncertainties is properly choosing source models and parameters. On the other hand, ranges of uncertainties are also investigated by calculating ΔCFS using different possible parameters. As described in the calculation of ΔCFS, the coseismic slip models of the 08YT (*Elliott et al.*, 2010) and 14YT (*Zhang et al.*, 2014) are chosen because they are the best choices for representative models of source slip distributions. For the 12YT, there is no other way to use a better source model than the synthetic slip model estimated from the empirical relations of *Wells and Coppersmith* (1994). The uncertainties due to different choices of friction coefficient and resolving depth are investigated (Tables S2-S3, Figures S5-S7). *Pollitz et al.* (2006) explored coseismic and postseismic stress changes following the 26 December 2004 Sumatra-Andaman and 28 March 2005 Nias earthquakes using different friction coefficients and found that the CFS changes are similar for values of μ' ranging from 0 to 0.8. In this study, a higher (0.8) or lower (0.2) value of the friction coefficient does not noticeabl influence the results of ΔCFS for this case (Tables S2 and S3, Figures S5 and S6). Calculations using different resolving depths (10 km and 15 km) show that the resolving depth also does not change the results of ΔCFS much (Figure S7). Thus, our conclusions based on ΔCFS are still valid considering the uncertainties. Because the focal mechanisms of the 20YT from different data sources (e.g., GCMT and NEIC-USGS) are similar, uncertainties of ΔCFS using different receiver fault parameters (strike, dip and rake) are small (Figure S8).

4.2 Validation of the Coulomb failure hypothesis

Stress interactions among multiple faults in a local-scale region provide a good opportunity to test the Coulomb failure hypothesis. Previous case studies have shown some successful examples from the view of stress transfer (*Freed and Lin*, 2001; *Jia et al.*, 2014; *Jia et al.*, 2018; *Pope and Mooney*, 2020; *Quigley et al.*, 2016). However, as mentioned above, calculations of ΔCFS suffer large uncertainties, and the results are subjective to some degree (e.g., choices of

source models and parameters are subjective). It is necessary to verify the results of ΔCFS from another perspective. Statistical insight (e.g., ETAS model) provides a good cross reference for its objectivity and small uncertainties. Background probabilities estimated from the formula (1) provide information on whether earthquakes are triggered aftershocks or tectonic background events. A low value (close to zero) of background probability indicates a triggered event, which usually experiences a positive ΔCFS induced by other major earthquakes. A high background probability value (close to 1.0) represents an independent event, which usually has no stress interaction with other earthquakes and results from tectonic loading. *Jia et al.* (2018) conducted a statistical analysis in the Jiuzhaigou region, southwestern China, to clarify the triggering relationship of the 2008 Wenchuan and 2017 Jiuzhaigou earthquakes, which cannot be well deduced from the results of ΔCFS . In this study, the background probability of the 12YT (0.97) coincides with the positive ΔCFS calculated on its hypocenter induced by the other major earthquakes (-1.5×10^{-4} MPa). Background probabilities of the 14YT (1.5×10^{-3}) and 20YT (8.7×10^{-5}) coincide with positive ΔCFS calculated on their hypocenters induced by the proceeding Yutian earthquakes (0.0036 MPa for the 14YT and 0.18 MPa for the 20YT). From these two different kinds of perspectives, the stress interaction among multiple faults or earthquakes can be comprehensively investigated.

5. Conclusion

The June 26, 2020 Mw 6.3 Yutian earthquake, which occurred on the western boundary of the Bayan Har block, is the fourth M6+ earthquake in this region since the occurrence of the 08YT. We have investigated the stress interaction among the 08YT, 12YT, 14YT and 20YT by applying the ETAS model and calculating ΔCFS . The joint application of these two independent methods provides insight into earthquake triggering mechanisms from both physics-based and statistics-based views in our study region and worldwide. From a statistical view, the background probabilities of the 08YT, 12YT, 14YT and 20YT are 0.87, 0.97, 1.5×10^{-3} and 8.7×10^{-5}, respectively, implying that the 08YT and 12YT are more similar to background earthquakes and that the 14YT and 20YT are triggered events. The epicenters of the 08YT, 12YT, 14YT and 20YT are located in the highest background seismicity areas (approximately 0.1 M≥3.5 events/degree^2/yr), which is a complex stepover zone with multiple

normal faults. From a physical view, the combined ΔCFS induced by the proceeding Yutian earthquakes on hypocenters of the 12YT, 14YT and 20YT are -1.50×10^{-4}, 3.6×10^{-3} and 1.5×10^{-1} MPa, respectively. These two kinds of evidence are consistent with each other, implying a triggering effect from the 08YT to the 14YT and the 20YT. Thus, a cross check of using the ETAS model and calculating ΔCFS together provides a robust and reliable way to investigate earthquake triggering mechanisms.

Acknowledgement

The catalog used in this study is from the China Earthquake Data Center (CEDC, http://data.earthquake.cn/index.html). The PSGRN/PSCMP code is provided by Prof. Rongjiang Wang. We benefit from discussion with Fuqiang Shi and Hurong Duan. We appreciate the comments and suggestions of two anonymous reviewers and the editor Lucy Flesch, which greatly improved this article. This research is jointly supported by the National Key R&D Program of China (2018YFC1503400), the National Natural Science Foundation of China projects (41804048, U2039204), the China Seismic Experimental Site (2019CSES0106), the China Postdoctoral Science Foundation (2020M673469), and the Fundamental Research Funds for the Central Universities (3102019ZDHKY12). Generic Mapping Tool mapping software (*Wessel and Smith*, 1991) is used to prepare some figures.

References

Agata, R., S. D. Barbot, K. Fujita, M. Hyodo, T. Iinuma, R. Nakata, T. Ichimura, and T. Hori (2019), Rapid mantle flow with power-law creep explains deformation after the 2011 Tohoku mega-quake, *Nature communications*, *10*(1), 1-11.

Bie, L., and I. Ryder (2014), Recent seismic and aseismic activity in the Ashikule stepover zone, NW Tibet, *Geophysical Journal International*, *198*(3), 1632-1643.

Cattania, C., S. Hainzl, L. Wang, B. Enescu, and F. Roth (2015), Aftershock triggering by postseismic stresses: A study based on Coulomb rate‐and‐state models, *Journal of Geophysical Research: Solid Earth*, *120*(4), 2388-2407.

Elliott, J. R., R. J. Walters, P. C. England, J. A. Jackson, Z. Li, and B. Parsons (2010), Extension on the Tibetan plateau: recent normal faulting measured by InSAR and body wave seismology, *Geophysical Journal International*, *183*(2), 503–535.

Freed, A. M. (2005), Earthquake triggering by static, dynamic, and postseismic stress transfer, *Annu. Rev. Earth Planet. Sci.*, *33*, 335-367.

Freed, A. M. (2007), Afterslip (and only afterslip) following the 2004 Parkfield, California, earthquake, *Geophysical Research Letters*, *34*(6).

Freed, A. M., and J. Lin (2001), Delayed triggering of the 1999 Hector Mine earthquake by viscoelastic stress transfer, *Nature*, *411*(6834), 180-183, doi:10.1038/35075548.

Gomberg, J., P. Reasenberg, P. l. Bodin, and R. Harris (2001), Earthquake triggering by seismic waves following the Landers and Hector Mine earthquakes, *Nature*, *411*(6836), 462-466.

Harris, R. A. (1998), Introduction to Special Section: Stress Triggers, Stress Shadows, and Implications for Seismic Hazard, *Journal of Geophysical Research*, *103*(10), 24347-24358.

Harris, R. A., and R. W. Simpson (1996), In the shadow of 1857-the effect of the Great Ft. Tejon Earthquake on subsequent earthquakes in southern California, *Geophysical Research Letters*, *23*(3), 229–232.

He, P., M. Wang, Q. Wang, and Z. Shen (2018), Rheological structure of lithosphere in northern Tibet inferred from postseismic deformation modeling of the 2001 Mw 7. 8 Kokoxili earthquake, *Chinese Journal of Geophysics-Chinese Edition*, *61*(2), 531-544.

He, P., Y. Wen, K. Ding, and C. Xu (2020), Normal Faulting in the 2020 Mw 6.2 Yutian Event: Implications for Ongoing E–W Thinning in Northern Tibet, *Remote Sensing*, *12*(18), 3012.

Helmstetter, A., and B. E. Shaw (2009), Afterslip and aftershocks in the rate‐and‐state friction law, *Journal of Geophysical Research: Solid Earth*, *114*(B1).

Hill, D., and S. Prejean (2007), Dynamic triggering, *Treatise on Geophysics*, *4*, 257-292.

Hughes, K. L., T. Masterlark, and W. D. Mooney (2010), Poroelastic stress-triggering of the 2005 M8. 7 Nias earthquake by the 2004 M9. 2 Sumatra–Andaman earthquake, *Earth and Planetary Science Letters*, *293*(3-4), 289-299.

Jia, K., S. Zhou, and R. Wang (2012), Stress Interactions within the Strong Earthquake Sequence from 2001 to 2010 in the Bayankala Block of Eastern Tibet, *Bulletin of the Seismological Society of America*, *102*(5), 2157-2164.

Jia, K., S. Zhou, J. Zhuang, and C. Jiang (2014), Possibility of the Independence between the 2013 Lushan Earthquake and the 2008 Wenchuan Earthquake on Longmen Shan Fault, Sichuan, China, *Seismological Research Letters*, *85*(1), 60-67, doi:10.1785/0220130115.

Jia, K., S. Zhou, J. Zhuang, C. Jiang, Y. Guo, Z. Gao, and S. Gao (2018), Did the 2008 Mw 7.9 Wenchuan earthquake trigger the occurrence of the 2017 Mw 6.5 Jiuzhaigou earthquake in Sichuan, China?, *Journal of Geophysical Research: Solid Earth*, *123*(4), 2965-2983.

Jiang, C., L. Han, and L. Guo (2014), Parameter Characteristics in the Early Period of Three Earthquake Sequences in the Yutian, Xiniiang Since 2008, *Acta Seis-mologiea Sinica*, *36*(2), 165-174.

Jonsson, S., P. Segall, R. Pedersen, and G. Björnsson (2003), Post-earthquake ground movements correlated to pore-pressure transients, *Nature*, *424*(6945), 179-183.

Kroll, K. A., K. B. Richards‐Dinger, J. H. Dieterich, and E. S. Cochran (2017), Delayed seismicity rate changes controlled by static stress transfer, *Journal of Geophysical Research: Solid Earth*, *122*(10), 7951-7965.

Li, Y., L. Chen, S. Liu, S. Yang, X. Yang, and G. Zhang (2015), Coseismic Coulomb stress changes caused by the Mw6.9 Yutian earthquake in 2014 and its correlation to the 2008 Mw7.2 Yutian earthquake, *Journal of Asian Earth Sciences*, *105*, 468-475.

Liu, S., Z.-K. Shen, R. Bürgmann, and S. Jónsson (2021), Thin crème brûlée rheological structure for the Eastern California Shear Zone, *Geology*, *49*(2), 216-221.

Masuti, S., S. D. Barbot, S. I. Karato, L. Feng, and P. Banerjee (2016), Upper-mantle water stratification

474 inferred from observations of the 2012 Indian Ocean earthquake, *Nature*, *538*(7625), 373.
475 McCloskey, J., S. S. Nalbant, and S. Steacy (2005), Earthquake risk from co-seismic stress, *Nature*,
476 *434*(7031), 291-291.
477 Meng, X., and Z. Peng (2014), Seismicity rate changes in the Salton Sea Geothermal Field and the San
478 Jacinto Fault Zone after the 2010 Mw 7.2 El Mayor-Cucapah earthquake, *Geophysical Journal*
479 *International*, *197*(3), 1750-1762.
480 Nur, A., and G. Mavko (1974), Postseismic Viscoelastic Rebound, *Science*, *183*(4121), 204-206.
481 Ogata, Y. (1998), Space-Time Point-Process Models for Earthquake Occurrences, *Annals of the Institute*
482 *of Statistical Mathematics*, *50*(2), 379-402, doi:10.1023/A:1003403601725.
483 Ogata, Y. (2004), Space-time model for regional seismicity and detection of crustal stress changes,
484 *Journal of Geophysical Research*, *109*(B3), 235-273.
485 Ogata, Y., and J. Zhuang (2006), Space–time ETAS models and an improved extension, *Tectonophysics*,
486 *413*(1–2), 13-23, doi:10.1016/j.tecto.2005.10.016.
487 Parsons, T. (2002), Global Omori law decay of triggered earthquakes: Large aftershocks outside the
488 classical aftershock zone, *Journal of Geophysical Research*, *107*(B9), 2199, doi:10.1029/2001JB000646.
489 Peña, C., O. Heidbach, M. Moreno, J. Bedford, M. Ziegler, A. Tassara, and O. Oncken (2019), Role of
490 lower crust in the postseismic deformation of the 2010 Maule earthquake: Insights from a model with
491 power-law rheology, *Pure and Applied Geophysics*, *176*(9), 3913-3928.
492 Peña, C., O. Heidbach, M. Moreno, J. Bedford, M. Ziegler, A. Tassara, and O. Oncken (2020), Impact of
493 power-law rheology on the viscoelastic relaxation pattern and afterslip distribution following the 2010
494 Mw 8.8 Maule earthquake, *Earth and Planetary Science Letters*, *542*, 116292.
495 Pollitz, F. F., P. Banerjee, R. Bürgmann, M. Hashimoto, and N. Choosakul (2006), Stress changes along
496 the Sunda trench following the 26 December 2004 Sumatra‐Andaman and 28 March 2005 Nias
497 earthquakes, *Geophysical research letters*, *33*(6).
498 Pollitz, F. F., and C. Cattania (2017), Connecting crustal seismicity and earthquake‐driven stress
499 evolution in Southern California, *Journal of Geophysical Research: Solid Earth*, *122*(8), 6473-6490.
500 Pope, N., and W. D. Mooney (2020), Coulomb stress models for the 2019 Ridgecrest, California
501 earthquake sequence, *Tectonophysics*, *791*, 228555.
502 Quigley, M. C., M. W. Hughes, B. A. Bradley, S. van Ballegooy, C. Reid, J. Morgenroth, T. Horton, B.
503 Duffy, and J. R. Pettinga (2016), The 2010–2011 Canterbury earthquake sequence: Environmental effects,
504 seismic triggering thresholds and geologic legacy, *Tectonophysics*, *672*, 228-274.
505 Ramos, M. D., J. C. Neo, P. Thakur, Y. Huang, and S. Wei (2020), Stress Changes on the Garlock fault
506 during and after the 2019 Ridgecrest Earthquake Sequence, *Bulletin of the Seismological Society of*
507 *America*.
508 Reasenberg, P. A., and R. W. Simpson (1992), Response of regional seismicity to the static stress change
509 produced by the loma prieta earthquake, *Science*, *255*(5052), 1687.
510 Steacy, S., J. Gomberg, and M. Cocco (2005), Introduction to special section: Stress transfer, earthquake
511 triggering, and time-dependent seismic hazard, *Journal of Geophysical Research*, *110*(B5),
512 doi:10.1029/2005JB003692.
513 Steacy, S., D. Marsan, S. S. Nalbant, and J. McCloskey (2004), Sensitivity of static stress calculations to
514 the earthquake slip distribution, *Journal of Geophysical Research: Solid Earth (1978–2012)*, *109*(B4).
515 Stein, R. S. (1999), The role of stress transfer in earthquake occurrence, *Nature*, *402*(6762), 605-609,
516 doi:10.1038/45144.
517 Tapponnier, P., X. Zhiqin, F. Roger, B. Meyer, N. Arnaud, G. Wittlinger, and Y. Jingsui (2001), Oblique

stepwise rise and growth of the Tibet Plateau, *science*, *294*(5547), 1671-1677.
Taylor, M., and A. Yin (2009), Active structures of the Himalayan-Tibetan orogen and their relationships to earthquake distribution, contemporary strain field, and Cenozoic volcanismActive structures on the Tibetan plateau and surrounding regions, *Geosphere*, *5*(3), 199-214.
Toda, S., R. S. Stein, G. C. Beroza, and D. Marsan (2012), Aftershocks halted by static stress shadows, *Nature Geoscience*, *5*(6), 410-413.
Toda, S., R. S. Stein, K. Richards-Dinger, and S. B. Bozkurt (2005), Forecasting the evolution of seismicity in southern California: Animations built on earthquake stress transfer, *Journal of Geophysical Research*, *110*(B5), doi:10.1029/2004JB003415.
Tung, S., and T. Masterlark (2018), Delayed poroelastic triggering of the 2016 October Visso earthquake by the August Amatrice earthquake, Italy, *Geophysical Research Letters*, *45*(5), 2221-2229.
Wan, Y., and Z.-K. Shen (2010), Static Coulomb stress changes on faults caused by the 2008 Mw 7.9 Wenchuan, China earthquake, *Tectonophysics*, *491*(1–4), 105-118, doi:10.1016/j.tecto.2010.03.017.
Wang, J., C. Xu, J. T. Freymueller, and Z. Li (2017), Probing Coulomb stress triggering effects for a Mw > 6.0 earthquake sequence from 1997 to 2014 along the periphery of the Bayan Har block on the Tibetan Plateau, *Tectonophysics*, *694*, 249-267, doi:https://doi.org/10.1016/j.tecto.2016.11.009.
Wang, J., C. Xu, J. T. Freymueller, Z. Li, and W. Shen (2014a), Sensitivity of Coulomb stress change to the parameters of the Coulomb failure model: A case study using the 2008 M w 7.9 Wenchuan earthquake, *Journal of Geophysical Research*, *119*(4), 3371–3392.
Wang, K., and Y. Fialko (2018), Observations and Modeling of Coseismic and Postseismic Deformation Due To the 2015 Mw 7.8 Gorkha (Nepal) Earthquake, *Journal of Geophysical Research Solid Earth*.
Wang, R., F. Lorenzo-Martín, and F. Roth (2006), PSGRN/PSCMP—A new code for calculating co-and post-seismic deformation, geoid and gravity changes based on the viscoelastic-gravitational dislocation theory, *Computers and Geosciences*, *32*(4), 527-541.
Wang, Y., F. Wang, M. Wang, Z. K. Shen, and Y. Wan (2014b), Coulomb Stress Change and Evolution Induced by the 2008 Wenchuan Earthquake and its Delayed Triggering of the 2013 Mw 6.6 Lushan Earthquake, *Seismological Research Letters*, *85*(1), 52-59.
Wells, D. L., and K. J. Coppersmith (1994), New empirical relationships among magnitude, rupture length, rupture width, rupture area, and surface displacement, *Bulletin of the seismological Society of America*, *84*(4), 974-1002.
Wessel, P., and W. H. F. Smith (1991), Free software helps map and display data, *Eos Trans. AGU*, *72*(41), 441-446, doi:10.1029/90eo00319.
Xiong, X., B. Shan, Y. Zheng, and R. Wang (2010), Stress transfer and its implication for earthquake hazard on the Kunlun Fault, Tibet, *Tectonophysics*, *482*(1–4), 216-225, doi:10.1016/j.tecto.2009.07.020.
Xu, X., X. Tan, G. Yu, G. Wu, W. Fang, J. Chen, H. Song, and J. Shen (2013), Normal-and oblique-slip of the 2008 Yutian earthquake: evidence for eastward block motion, northern Tibetan Plateau, *Tectonophysics*, *584*, 152-165.
Zhang, P., Q. Deng, G. Zhang, J. Ma, W. Gan, W. Min, F. Mao, and Q. Wang (2003), Active tectonic blocks and strong earthquakes in the continent of China, *Science in China Series D: Earth Sciences (in Chinese)*, *46*(2), 13-24.
Zhang, Y., L.-s. Xu, Y.-T. Chen, and R.-j. Wang (2014), Fast inversion for the rupture process of the 12 February 2014 Yutian MW6. 9 earthquake: Discussion on the impacts of focal mechanisms on rupture process inversions, *Acta Seismologica Sinica*, *36*(2), 159-164.
Zhao, L., L. Zhao, and X. Xie (2016), Static Coulomb stress changes and seismicity rate in the source

562 region of the 12 February, 2014 M W 7.0 Yutian earthquake in Xinjiang, China, *Chinese Journal of*
563 *Geophysics*, 3732-3743.
564 Zhuang, J., C.-P. Chang, Y. Ogata, and Y.-I. Chen (2005), A study on the background and clustering
565 seismicity in the Taiwan region by using point process models, *J. Geophys. Res.*, *110*(B5),
566 doi:10.1029/2004jb003157.
567 Zhuang, J., Y. Ogata, and D. Vere-Jones (2004), Analyzing earthquake clustering features by using
568 stochastic reconstruction, *Journal of Geophysical Research: Solid Earth*, *109*(B5), B05301,
569 doi:10.1029/2003JB002879.
570